Calculation of stresses in InxGa1-xAs/InP strained multilayer heterostructures

著者	中嶋　一雄
journal or publication title	Journal of Applied Physics
volume	72
number	11
page range	5213-5219
year	1992
URL	http://hdl.handle.net/10097/47322

doi: 10.1063/1.352003

Calculation of stresses in $In_xGa_{1-x}As/InP$ strained multilayer heterostructures

Kazuo Nakajima
Fujitsu Laboratories Limited, Atsugi, Morinosato-Wakamiya 10-1, Atsugi 243-01, Japan

(Received 26 April 1991; accepted for publication 17 August 1992)

A theoretical model was proposed to calculate the stress in the multilayer heterostructures such as multiple quantum well and strained quantum well structures. The model was derived under consideration of the difference between crystalline parameters such as the lattice constant and thermal expansion coefficient of the composed crystal layers. In this model, each composed crystal layer is divided into many imaginary thin layers. The face force and strain balance was considered over all the imaginary thin layers with coherent interfaces. Using this model, the stress in the lattice-matched $InP/In_{0.53}Ga_{0.47}As$ and strained $InP/In_{0.82}Ga_{0.18}As$ multilayer heterostructures was calculated at 600 °C. In the multilayer, the compressive stress in the $In_{0.53}Ga_{0.47}As$ and $In_{0.82}Ga_{0.18}As$ layers is always larger than the tensile stress in the InP layers. The stress in the $In_xGa_{1-x}As$ layers decreases as the thickness of the $In_xGa_{1-x}As$ layers increases, and it increases by adding InP thick layers on the one side or both sides of the multilayer. The tangential and perpendicular lattice constants in the multilayer were calculated using this model. The perturbation of the InP lattice becomes smaller and that of the InGaAs lattice becomes larger by adding the thick InP layers. It is found from these results that the total stress at the InP/InGaAs heterointerface depends on only the lattice misfit, but the share of the total stress depends strongly on the structure.

I. INTRODUCTION

Multilayer heterostructures are important for fabricating multiple quantum well (MQW) and strained quantum well (SQW) structures. However, the stress caused by lattice misfit and thermal strain has not been accurately calculated in the MQW and SQW structures. In the calculation of stresses in heterostructures composed of crystals with different lattice constants and thermal expansion coefficients such as III-V compounds, the difference between crystalline parameters such as the lattice constant and thermal expansion coefficient of composed crystal layers must be taken into consideration. Calculation models of stress distribution in heterostructures have been reported by several researchers,[1–5] but each layer has been regarded as only a strip and the difference between lattice constants have not been considered in their model.

Chu *et al.*[6] and Cembali and Servidori[7] have reported the stress calculation model for multilayer heterostructures under consideration of the difference of lattice constants. Their model is based on Davidenkov's expression[8] of the bending moment. Their model is useful for the uniformly bending heterostructure with a very thick layer such as a substrate. However, they cannot be applied for the symmetric heterostructures without a very thick layer and the irregularly bending heterostructures, and the thermal expansion coefficient is not taken into account in their model.

In this work, an improved calculation model of stress distribution in multilayer heterostructures is derived under consideration of the difference between crystalline parameters such as the lattice constant and thermal expansion coefficient of the crystalline layers. In this model, each layer is divided into many imaginary thin layers,[9] and the face force and strain balance is considered over the all imaginary thin layers with coherent interfaces. The stress distribution in the multilayer heterostructures can be precisely calculated by this model. Using this calculation model, the stress distribution in $In_xGa_{1-x}As/InP$ strained multilayer heterostructures with various lattice misfits and layer thicknesses is calculated, and the distribution of the lattice constant in the heterostructures is calculated. The temperature used for the calculation is 600 °C at which $In_xGa_{1-x}As$ is generally grown on InP.

II. CALCULATION METHOD

The schematic geometry of a multilayer heterostructure is given in Fig. 1. The length of each layer before deformation is Na_1, Na_2, and Na_3, where a_1, a_2, and a_3 are the lattice constants and N is the number of the unit cells of the layers, and the thickness of each layer is t_1, t_2, and t_3 as shown in Fig. 1(a). It is considered that each layer consists of many imaginary thin layers. The total number of imaginary thin layers is g. The ith imaginary thin layer has a layer thickness of d_i, a thermal expansion coefficient of α_i, a Young's modulus of E_i, a Poisson's ratio of ν_i, and a lattice constant of a_i. The length of the ith imaginary thin layer is $Na_i^{\parallel}$, where $a_i^{\parallel}$ is the tangential lattice constant of the ith layer. Each layer has coherent interfaces with both neighboring layers as shown in Fig. 1(b). Such a layer experiences a face force F_i and a moment M_i. The multilayer heterostructure is transformed from Fig. 1(a) to Fig. 1(b) because of their coherency at a temperature, T.

According to the balance of general forces and moments, we have

$$\sum_{i=1}^{g} F_i=0, \tag{1}$$

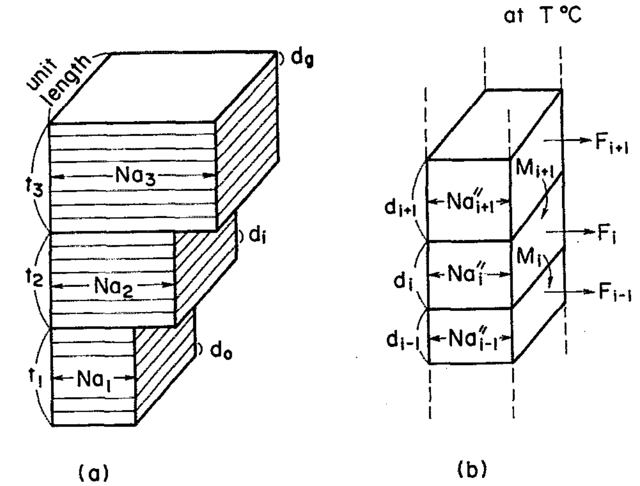

FIG. 1. Schematic geometry of the multilayer heterostructures consisting of imaginary thin layers: (a) structure before perturbation and (b) perturbed structure with coherent interfaces.

$$\sum_{i=1}^{g} M_i+\sum_{i=1}^{g} F_i\left(\sum_{j<i} d_j+\frac{d_i}{2}\right)=0, \tag{2}$$

where

$$M_i=\frac{E_i I_i}{R}=\frac{E_i d_i^3}{12R}, \tag{3}$$

where F_i is the face force per unit length of the ith imaginary thin layer, R is the curvature radius, and I_i is the moment of inertia of the ith imaginary thin layer. At the interface between the top of the ith imaginary thin layer and the bottom of the $(i+1)$th imaginary thin layer, the tangential lengths per unit lattice constant should be equal because of their coherency:

$$l_i+\frac{a_i F_i}{E_i d_i}+\frac{a_i d_i}{2R}=l_{i+1}+\frac{a_{i+1}F_{i+1}}{E_{i+1}d_{i+1}}-\frac{a_{i+1}d_{i+1}}{2R} \quad (i<g), \tag{4}$$

where

$$l_i=a_i(1+\alpha_i T), \tag{5}$$

and $d_i/2R$ is the strain per unit length caused by bending. As shown in the Appendix, using Eqs. (1) and (4), we have

$$F_i=E_i\, d_i/a_i \sum_{j=1}^{g}\left(\frac{E_j d_j}{a_j}\right)\left[\frac{1}{R}\sum_{j=1}^{g}\left(\frac{E_j d_j}{a_j}\right)\left(\sum_{k<i} a_k d_k-\sum_{k<j} a_k d_k+\frac{a_i d_i-a_j d_j}{2}\right)+\sum_{j=1}^{g}\left(\frac{E_j d_j}{a_j}\right)(l_j-l_i)\right]. \tag{6}$$

Substituting Eq. (6) into Eqs. (2) and (3), we have

$$\frac{1}{R}=\frac{R_3}{R_1+R_2}, \tag{7}$$

where

$$R_1=\sum_{l=1}^{g}\left(\frac{E_l d_l}{a_l}\right)\sum_{i=1}^{g} E_i d_i^3, \tag{8}$$

$$R_2=3\sum_{i=1}^{g}\left(\frac{E_i d_i}{a_i}\right)\left(2\sum_{j<i} d_j+d_i\right)\sum_{j=1}^{g}\left(\frac{E_j d_j}{a_j}\right)\times\left(2\sum_{k<i} a_k d_k-2\sum_{k<j} a_k d_k+a_i d_i-a_j d_j\right), \tag{9}$$

$$R_3=6\sum_{i=1}^{g}\left(\frac{E_i d_i}{a_i}\right)\left(2\sum_{j<i} d_j+d_i\right)\sum_{j=1}^{g}\left(\frac{E_j d_j}{a_j}\right)(l_i-l_j). \tag{10}$$

In the previously reported calculation methods,[1-5] the difference between lattice constants of the ith and $(i+1)$th layers is not considered and the lattice constants a_i and a_{i+1} are assumed to be equal. However, in the present calculation model shown by Eqs. (6) and (7), the difference between the lattice constants a_i and a_{i+1} is taken into account.

Under the condition that the thickness of all the imaginary thin layers are the same, we obtain the following equations for F_i and R:

$$F_i=E_i\, d/a_i \sum_{j=1}^{g}\left(\frac{E_j}{a_j}\right)\left[\frac{d}{R}\sum_{j=1}^{g}\left(\frac{E_j}{a_j}\right)\left(\sum_{k<i} a_k-\sum_{k<j} a_k+\frac{a_i-a_j}{2}\right)+\sum_{j=1}^{g}\left(\frac{E_j}{a_j}\right)(l_j-l_i)\right], \tag{11}$$

$$\frac{1}{R}=\frac{6\Sigma_{i=1}^{g}(E_i/a_i)(2_i-1)\Sigma_{j=1}^{g}(E_j/a_j)(l_i-l_j)}{d[\Sigma_{l=1}^{g}(E_l/a_l)\Sigma_{i=1}^{g}E_i+3\Sigma_{i=1}^{g}(E_i/a_i)(2i-1)\Sigma_{j=1}^{g}(E_j/a_j)(2\Sigma_{k<i}a_k-2\Sigma_{k<j}a_k+a_i-a_j]}. \tag{12}$$

where d is the thickness of the imaginary thin layer. The strain per unit length in the ith imaginary thin layer at temperature, T, is given by the sum of the strain due to the force, F_i, plus the bending strain as follows:

$$S_i=\frac{F_i}{E_i d_i}+\frac{d_i}{2R}. \tag{13}$$

The stress per unit area in the ith imaginary thin layer at the temperature, T, is given using Eq. (13) as follows:

$$\sigma_i=E_i S_i=\frac{F_i}{d_i}+\frac{E_i d_i}{2R}. \tag{14}$$

This model can be used for the calculation of the stress

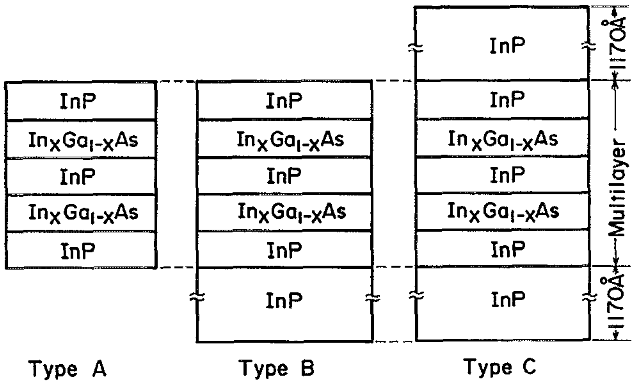

FIG. 2. InP/$In_xGa_{1-x}As$ multilayer heterostructures used in the calculation: (a) multilayer, (b) multilayer on a thick InP layer, and (c) multilayer between thick InP layers.

distribution in all types of crystalline structures such as the compositionally graded layer and strained multilayer heterostructures.

From Eqs. (4) and (5), the tangential lattice constant, $a_i^{\parallel}$, and the perpendicular lattice constant, $a_i^{\perp}$, of the ith imaginary thin layer are given as follows:

$$a_i^{\parallel}=a_i\left(1+\alpha_i T+\frac{F_i}{E_i d_i}+\frac{d_i}{2R}\right), \tag{15}$$

and

$$a_i^{\perp}=a_i\left[1+C_i\left(\alpha_i T+\frac{F_i}{E_i d_i}+\frac{d_i}{2R}\right)\right], \tag{16}$$

where

$$C_i=-2\nu_i/(1-\nu_i). \tag{17}$$

In these equations, the positive and negative values for F_i, S_i, and E_iS_i signify the tensile and compressive ones, respectively.

III. CALCULATED RESULTS

A Parameters used in the calculation

The stress and lattice constant distributions were calculated for the three types of InP/$In_xGa_{1-x}As$ multilayer heterostructures as shown in Fig. 2. The structure of type A is composed of only the multilayer, that of type B is composed of the multilayer on a thick InP layer, and that of type C is composed of the multilayer with thick InP layers on both sides. The calculation was performed for two kinds of the multilayer such as the lattice matched type of InP/$In_{0.53}Ga_{0.47}As$ and the strained type of InP/$In_{0.82}Ga_{0.18}As$.

Young's modulus for GaAs, InAs, and InP are estimated as 0.853×10^{12}, 0.505×10^{12}, and 0.607×10^{12} dyn/cm^2, respectively, using Brantly's equation[10] and elastic stiffnesses.[11–13] Young's modulus of $In_{0.53}Ga_{0.47}As$ and $In_{0.82}Ga_{0.18}As$ are derived from these values as 0.668×10^{12} and 0.568×10^{12} dyn/cm^2, respectively, on the assumption of its linearity for composition.

The Poisson ratios for GaAs, InAs, and InP are estimated as 0.31, 0.36, and 0.35, respectively, using elastic compliance constants.[11–13] The Poisson ratios of $In_{0.53}Ga_{0.47}As$ and $In_{0.82}Ga_{0.18}As$ are derived from these values as 0.336 and 0.35, respectively, on the assumption of its linearity for composition.

The lattice constant of InP is 5.86875 Å[14] and that of $In_{0.82}Ga_{0.18}As$ is 5.9861 Å, which is estimated from those of GaAs (5.6535 Å)[15] and InAs (6.0584 Å)[14] using Vergard's law. The lattice misfit, $\Delta a/a$, between InP and $In_{0.82}Ga_{0.18}As$ is 0.02, where Δa is equal to the lattice constant of InGaAs minus the lattice constant of InP, a. The thermal expansion coefficient of InP is 4.56×10^{-6}/°C[16] and that of $In_{0.82}Ga_{0.18}As$ is estimated as 4.0×10^{-6}/°C from those of GaAs (6.86×10^{-6}/°C)[17] and $In_{0.53}Ga_{0.47}As$ (5.66×10^{-6}/°C).[16]

In this work, these values of the crystalline parameters of InP are used for E_i, ν_i, a_i, and α_i in the InP layers, and those of $In_{0.53}Ga_{0.47}As$ and $In_{0.82}Ga_{0.18}As$ are used for E_i, ν_i, a_i, and α_i in the $In_{0.53}Ga_{0.47}As$ and $In_{0.82}Ga_{0.18}As$ layers, respectively. So, these original parameters are constant inside each layer.

B. Stress and lattice constant distributions

The stress at 600 °C was calculated for $d_i=2a_i$ using Eqs. (6), (7), and (14). When the crystalline parameters vary inside each layer, the stress distribution inside each layer can be more precisely calculated when a smaller d_i is adopted. However, when the crystalline parameters are constant inside each layer such as this case, the calculated results are not sensitive to variation in d_i. For example, the calculated results for $d_i=2a_i$ and $d_i=4a_i$ are almost equal to each other. Even in this case, the precise stress distribution can be known using many imaginary thin layers as shown in the calculated results for the InP/InGaAs multilayer on a thick InP layer.

The total number of imaginary thin layers, g, depends on the structure. In this calculation, $g=40$ was used for the InP 117 Å/$In_{0.53}Ga_{0.47}As$ 59 Å and InP 117 Å/$In_{0.82}Ga_{0.18}As$ 60 Å structures, and $g=50$ was used for the InP 117 Å/$In_{0.53}Ga_{0.47}As$ 117 Å and InP 117 Å/$In_{0.82}Ga_{0.18}As$ 120 Å structures. When a 1170-Å-thick InP layer was added to the multilayer, 100 was added to g. Therefore, $g=250$ was used for the strained structure of the InP 117 Å/$In_{0.82}Ga_{0.18}As$ 120 Å multilayer between 1170-Å-thick InP layers.

Figures 3, 4, and 5 show the stress at 600 °C in the three types of InP/$In_{0.53}Ga_{0.47}As$ multilayer heterostructures which are lattice matched at room temperature, and Figs. 3, 4, and 5 correspond to the calculated results for types A, B, and C, respectively, as shown in Fig. 2. The positive and negative stresses are tensile and compressive ones. The stress is shown as a function of the distance from the bottom of the multilayer heterostructures. In Figs. 3, 4, and 5, lines a and b correspond to the calculated results for the InP 117 Å/$In_{0.53}Ga_{0.47}As$ 59 Å, and InP 117 Å/$In_{0.53}Ga_{0.47}As$ 117 Å multilayers, respectively. The multilayer in Fig. 4 is on a 1170-Å-thick InP layer and the

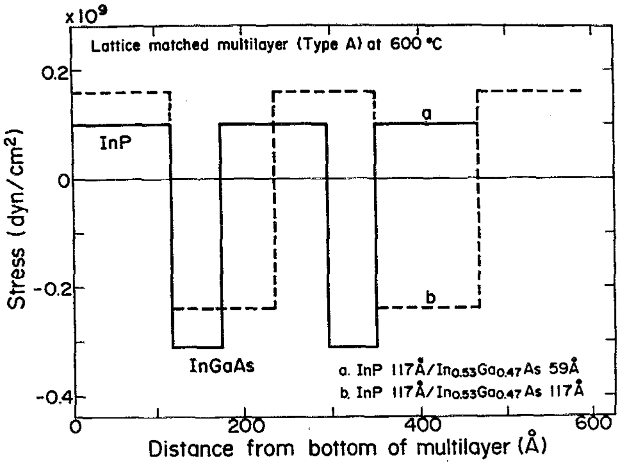

FIG. 3. Stress at 600 °C in the lattice-matched InP/$In_{0.53}Ga_{0.47}As$ multilayer (type A).

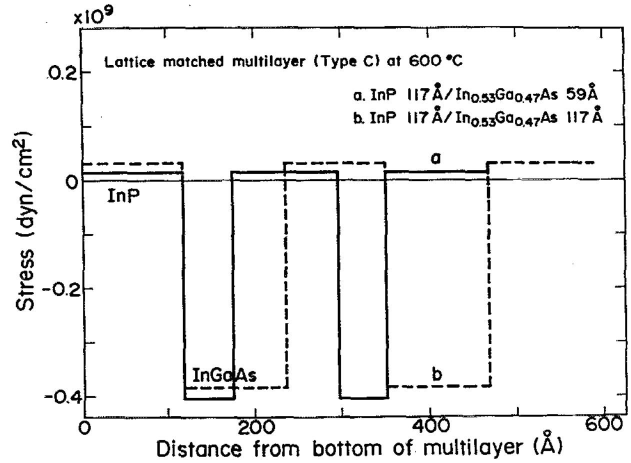

FIG. 5. Stress at 600 °C in the lattice-matched InP/$In_{0.53}Ga_{0.47}As$ multilayer between thick InP layers (type C).

multilayer in Fig. 5 is put between 1170-Å-thick InP layers. There are stresses in the lattice-matched multilayer because of the different thermal expansion coefficient. The stress in the $In_{0.53}Ga_{0.47}As$ layers is always larger than that in the InP layers. The stress in the $In_{0.53}Ga_{0.47}As$ layers decreases as the thickness of the $In_{0.53}Ga_{0.47}As$ layers increases. The stress in the $In_{0.53}Ga_{0.47}As$ layers increases and the stress in the InP layers decreases by adding the thick InP layers. In Fig. 5, the stress in the InP layers is almost zero. In Fig. 4, the stress in the $In_{0.53}Ga_{0.47}As$ layers decreases and the stress in the InP layers increases as the distance from the interface between the multilayer and the thick InP layer becomes larger. In Figs. 3 and 5, the stress in each layer is constant. Very large stress remains at the heterointerface.

Figures 6, 7, and 8 show the strêss at 600 °C in the three types of the strained multilayer heterostructures of InP/$In_{0.82}Ga_{0.18}As$, and Figs. 6, 7, and 8 correspond to the calculated results for the types A, B, and C, respectively, as shown in Fig. 2. Lines a and b correspond to the results for the InP 117 Å/$In_{0.82}Ga_{0.18}As$ 60 Å and InP 117Å/$In_{0.82}Ga_{0.18}As$ 120 Å multilayer, respectively. The multilayer in Fig. 7 is on a 1170-Å-thick InP layer and the multilayer in Fig. 8 is put between 1170-Å-thick InP layers. As compared with Figs. 3 and 6, the stress in the strained multilayer is about 30 times larger than that in the lattice-matched one. The stress in the $In_{0.82}Ga_{0.18}As$ layers is always larger than that in the InP layers. The stress in the $In_{0.82}Ga_{0.18}As$ layers decreases as the thickness of the $In_{0.82}Ga_{0.18}As$ layers increases. The stress in the $In_{0.82}Ga_{0.18}As$ layers slightly increases and the stress in the InP layers decreases by adding the thick InP layers. In Fig. 8, the stress in the InP layers is almost zero. In Fig. 4, the stress in the $In_{0.82}Ga_{0.18}As$ layers decreases and the stress in the InP layers increases as the distance from the interface between the multilayer and the thick InP layer becomes longer. In Figs. 6 and 8, the stress in each layer is constant. Very large stress remains at the strained heterointerface and throughout the ternary layer.

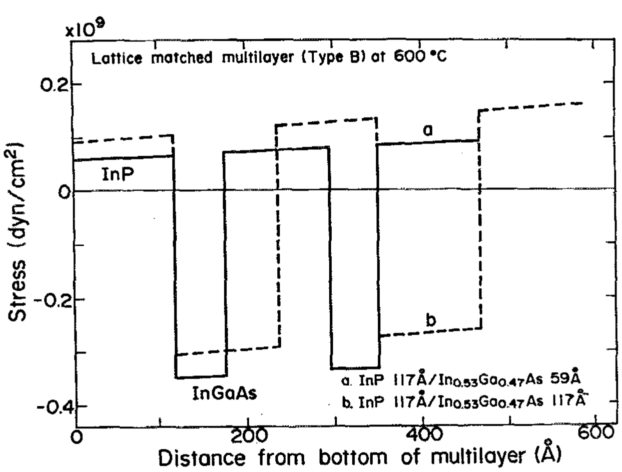

FIG. 4. Stress at 600 °C in the lattice-matched InP/$In_{0.53}Ga_{0.47}As$ multilayer on a thick InP layer (type B).

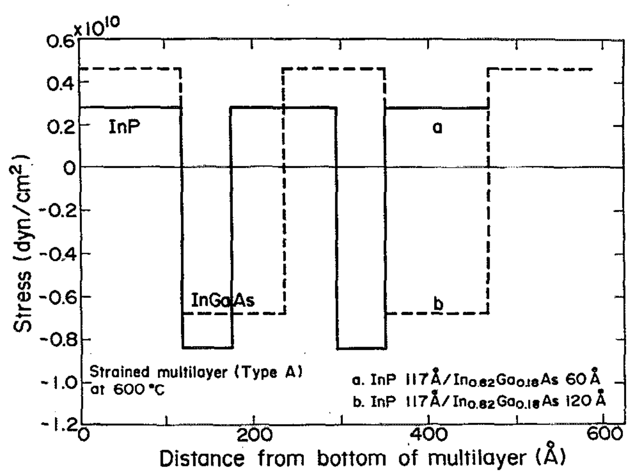

FIG. 6. Stress at 600 °C in the strained InP/$In_{0.82}Ga_{0.18}As$ multilayer (type A).

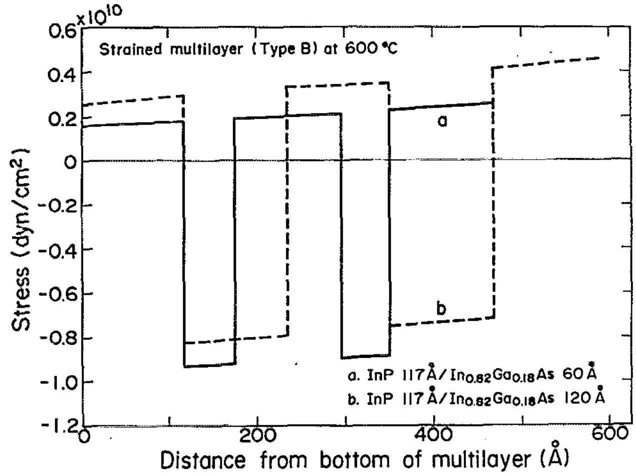

FIG. 7. Stress at 600 °C in the strained $InP/In_{0.82}Ga_{0.18}As$ multilayer on a thick InP layer (type B).

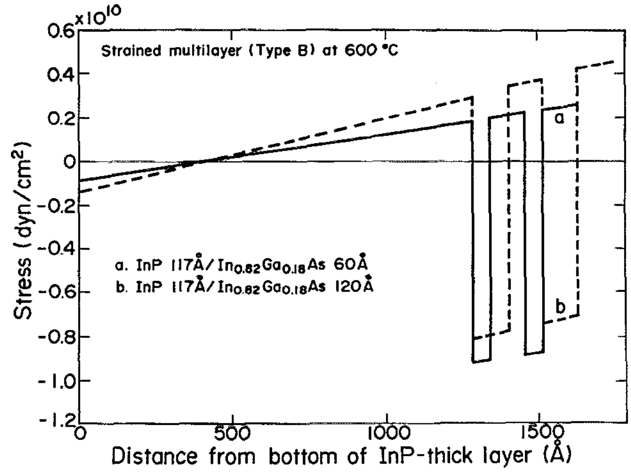

FIG. 9. Stress at 600 °C all over the structure of the strained $InP/In_{0.82}Ga_{0.18}As$ multilayer on a thick InP layer (type B).

Figure 9 shows the stress at 600 °C all over the type B structure of the $InP/In_{0.82}Ga_{0.18}As$ strained multilayer on the thick InP layer. Figure 7 shows only the multilayer and it is only a part of Fig. 9. The stress varies from compressive to tensile in the thick InP layer because of a bending s;train in it. The stress gradient in the thick InP layer increases as the thickness of the $In_{0.82}Ga_{0.18}As$ layer increases. The stress in the thick InP layer is smaller than that in the InP layer of the multilayer.

Figures 10 and 11 show the tangential and perpendicular lattice constants at 600 °C in the $InP/In_{0.82}Ga_{0.18}As$ strained multilayer of types A and C, respectively. The lattice constants were calculated for the InP 117 Å/$In_{0.82}Ga_{0.18}As$ 60 Å multilayer. The tangential lattice constant, $a^{\parallel}$, is constant over the multilayer and is between the original lattice constants of InP and $In_{0.82}Ga_{0.18}As$. The perpendicular lattice constant, $a^{\perp}$, of the InP layer becomes shorter than the original one because of the tensile stress in the InP lattice, and the perpendicular lattice constant of the $In_{0.82}Ga_{0.18}As$ layer becomes longer than the original one because of the compressive stress in the InGaAs lattice. As compared with Figs. 10 and 11, the tangential lattice constant of the multilayer comes near the original lattice constant of InP by adding the thick InP layers. The perpendicular lattice constant of the InP layer approaches the original lattice constant of InP, and the perpendicular lattice constant of the InGaAs layer becomes larger by adding the thick InP layers. This means that the perturbation of the InP lattice becomes smaller and that of the InGaAs lattice becomes larger by adding the thick InP layers.

IV. DISCUSSION

We know from these results that the InGaAs lattice is much more perturbed in the MQW and SQW InP/InGaAs structures grown on InP substrates. However, when the lattice misfit is constant, the total stress at the InP/InGaAs heterointerface is almost constant regardless of the existence of the thick InP layers as shown in Figs. 3–8. So, the

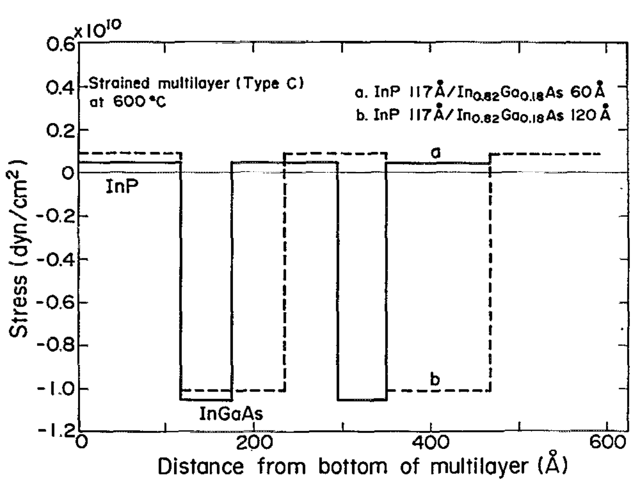

FIG. 8. Stress at 600 °C in the strained $InP/In_{0.82}Ga_{0.18}As$ multilayer between thick InP layers (type C).

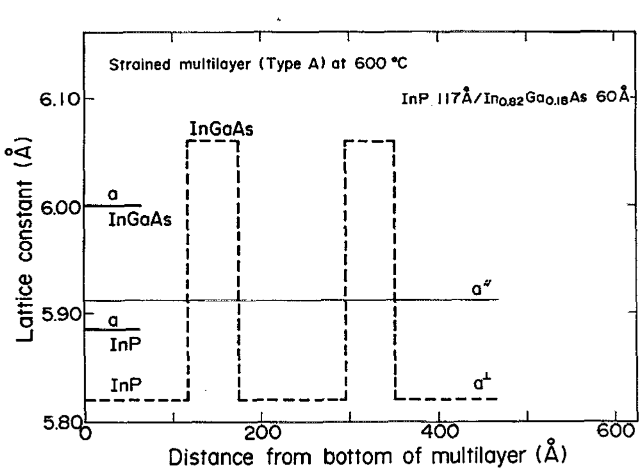

FIG. 10. Lattice constant at 600 °C in the strained $InP/In_{0.82}Ga_{0.18}As$ multilayer (type A).

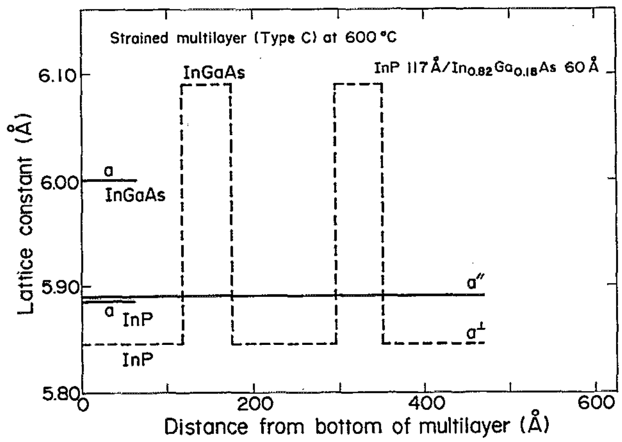

FIG. 11. Lattice constant at 600 °C in the strained InP/$In_{0.82}Ga_{0.18}As$ multilayer between thick InP layers (type C).

total stress depends on only the lattice misfit, but the share of the total stress depends strongly on the structure. In the MQW and SQW InP/InGaAs structures, the share of the total stress is very important, as it alters the dependence of the energy band structure on the stress in the InGaAs wells. Using this calculation model, we can know accurately the pure stress in the InGaAs wells of the MQW and SQW structures.

As shown in Fig. 9, we can accurately calculate the stress distribution in the thick InP layer by introduction of the concept of the imaginary thin layers and by consideration of the face force balance over all the imaginary thin layers. Using this model, we can know the precise stress distribution in all types of heterostructures.

V. SUMMARY

A theoretical model was proposed to calculate the stress in the multilayer heterostructures under consideration of the difference between crystalline parameters such as the lattice constant and thermal expansion coefficient of the crystalline layers. In this model, each crystal layer is divided into many imaginary thin layers and the face force balance is considered over all the imaginary thin layers with coherent interfaces.

Using this model, the stress was calculated in the lattice-matched InP/$In_{0.53}Ga_{0.47}As$ and strained InP/$In_{0.82}Ga_{0.18}As$ multilayer heterostructures at 600 °C. The stress in the $In_xGa_{1-x}As$ layers is always larger than that in the InP layers. The stress in the $In_xGa_{1-x}As$ layers decreases as the thickness of the $In_xGa_{1-x}As$ layers increases. The stress in the $In_xGa_{1-x}As$ layers increases and the stress in the InP layers decreases by adding the thick InP layers. It is found that the total stress at the InP/$In_xGa_{1-x}As$ heterointerface depends only on the lattice misfit, but the share of the total stress depends strongly on the structure.

The tangential and perpendicular lattice constants were calculated in the InP/$In_{0.82}Ga_{0.18}As$ strained multilayer heterostructures at 600 °C. The tangential lattice constant is constant over the multilayer, and it is between the original lattice constants of InP and $In_{0.82}Ga_{0.18}As$. The perpendicular lattice constant of the InP layer becomes shorter than the original one, and that of the $In_{0.82}Ga_{0.18}As$ layer becomes longer than the original one. The perturbation of the InP lattice is smaller than that of the $In_{0.82}Ga_{0.18}As$ lattice.

ACKNOWLEDGMENT

The author wishes to acknowledge the helpful discussion of N. Fujimura at the University of Osaka Prefecture.

APPENDIX

Eq. (6) can be derived using Eqs. (1) and (4). From Eq. (4), we have

$$
\begin{aligned}
&l_1+\frac{a_1F_1}{E_1d_1}+\frac{a_1d_1}{2R}=l_2+\frac{a_2F_2}{E_2d_2}-\frac{a_2d_2}{2R},\\
&l_2+\frac{a_2F_2}{E_2d_2}+\frac{a_2d_2}{2R}=l_3+\frac{a_3F_3}{E_3d_3}-\frac{a_3d_3}{2R},\\
&\vdots\\
&l_{i-1}+\frac{a_{i-1}F_{i-1}}{E_{i-1}d_{i-1}}+\frac{a_{i-1}d_{i-1}}{2R}=l_i+\frac{a_iF_i}{E_id_i}-\frac{a_id_i}{2R},\qquad\text{(A1)}\\
&l_i+\frac{a_iF_i}{E_id_i}+\frac{a_id_i}{2R}=l_{i+1}+\frac{a_{i+1}F_{i+1}}{E_{i+1}d_{i+1}}-\frac{a_{i+1}d_{i+1}}{2R},\\
&\vdots\\
&l_{g-1}+\frac{a_{g-1}F_{g-1}}{E_{g-1}d_{g-1}}+\frac{a_{g-1}d_{g-1}}{2R}=l_g+\frac{a_gF_g}{E_gd_g}-\frac{a_gd_g}{2R}.
\end{aligned}
$$

From Eq. (A1) we have

$$
\begin{aligned}
&F_1=\frac{E_1d_1}{a_1}(l_2-l_1)+\frac{a_2}{a_1}\frac{E_1d_1}{E_2d_2}F_2-\frac{1}{a_1}\frac{E_1d_1}{2R}(a_1d_1+a_2d_2),\\
&F_2=\frac{E_2d_2}{a_2}(l_3-l_2)+\frac{a_3}{a_2}\frac{E_2d_2}{E_3d_3}F_3-\frac{1}{a_2}\frac{E_2d_2}{2R}(a_2d_2+a_3d_3),\\
&\vdots\\
&F_{i-1}=\frac{E_{i-1}d_{i-1}}{a_{i-1}}(l_i-l_{i-1})+\frac{a_i}{a_{i-1}}\frac{E_{i-1}d_{i-1}}{E_id_i}F_i\\
&\qquad-\frac{1}{a_{i-1}}\frac{E_{i-1}d_{i-1}}{2R}(a_{i-1}d_{i-1}+a_id_i),\qquad\text{(A2)}\\
&F_{i+1}=\frac{E_{i+1}d_{i+1}}{a_{i+1}}(l_i-l_{i+1})+\frac{a_i}{a_{i+1}}\frac{E_{i+1}d_{i+1}}{E_id_i}F_i\\
&\qquad+\frac{1}{a_{i+1}}\frac{E_{i+1}d_{i+1}}{2R}(a_id_i+a_{i+1}d_{i+1}),\\
&\vdots\\
&F_g=\frac{E_gd_g}{a_g}(l_{g-1}-l_g)+\frac{a_{g-1}}{a_g}\frac{E_gd_g}{E_{g-1}d_{g-1}}F_{g-1}\\
&\qquad+\frac{1}{a_g}\frac{E_gd_g}{2R}(a_{g-1}d_{g-1}+a_gd_g).
\end{aligned}
$$

From Eq. (A2) we have

$$F_1=\frac{E_1d_1}{a_1}(l_2-l_1)+\frac{E_1d_1}{a_1}(l_3-l_2)+\frac{a_3}{a_1}\frac{E_1d_1}{E_3d_3}F_3$$

$$-\frac{1}{a_1}\frac{E_1d_1}{2R}(a_2d_2+a_3d_3)-\frac{1}{a_1}\frac{E_1d_1}{2R}(a_1d_1+a_2d_2)$$

$$=\frac{E_1d_1}{a_1}(l_i-l_1)+\frac{a_i}{a_1}\frac{E_1d_1}{E_i d_i}F_i-\frac{1}{a_1}\frac{E_1d_1}{R}$$

$$\times\left(\sum_{k<i}a_kd_k+\frac{a_i d_i-a_1d_1}{2}\right),$$

$$\vdots \tag{A3}$$

$$F_j=\frac{E_j d_j}{a_j}(l_i-l_j)+\frac{a_i}{a_j}\frac{E_j d_j}{E_i d_i}F_i-\frac{1}{a_j}\frac{E_j d_j}{R}$$

$$\times\left(\sum_{k<i}a_kd_k-\sum_{k<j}a_kd_k+\frac{a_i d_i-a_j d_j}{2}\right)(j<i),$$

$$F_j=F_i \quad (j=i),$$

$$F_j=\frac{E_j d_j}{a_j}(l_i-l_j)+\frac{a_i}{a_j}\frac{E_j d_j}{E_i d_i}F_i-\frac{1}{a_j}\frac{E_j d_j}{R}$$

$$\times\left(\sum_{k<i}a_kd_k-\sum_{k<j}a_kd_k+\frac{a_i d_i-a_j d_j}{2}\right)(j>i).$$

Substituting Eq. (A3) into Eq. (1), we have

$$\sum_{j=1}^{g}\frac{E_j d_j}{a_j}(l_i-l_j)+\frac{a_i F_i}{E_i d_i}\sum_{j=1}^{g}\frac{E_j d_j}{a_j}$$

$$-\sum_{j=1}^{g}\frac{E_j d_j}{a_j R}\left(\sum_{k<i}a_kd_k-\sum_{k<j}a_kd_k+\frac{a_i d_i-a_j d_j}{2}\right)=0. \tag{A4}$$

From Eq. (A4), we can have Eq. (6).

Eq. (7) can be derived using Eqs. (2), (3), and (6). Substituting Eqs. (3) and (6) into Eq. (2), we have

$$\sum_{i=1}^{g}\frac{E_i d_i^3}{12R}+\sum_{i=1}^{g}\left(\sum_{j<i}d_j+\frac{d_i}{2}\right)\left\{E_i d_i\Big/a_i\sum_{l=1}^{g}\frac{E_l d_l}{a_l}\right.$$

$$\times\left[\frac{1}{R}\sum_{j=1}^{g}\frac{E_j d_j}{a_j}\left(\sum_{k<i}a_kd_k-\sum_{k<j}a_kd_k+\frac{a_i d_i-a_j d_j}{2}\right)\right.$$

$$\left.\left.+\sum_{j=1}^{g}\frac{E_j d_j}{a_j}(l_j-l_i)\right]\right\}=0. \tag{A5}$$

From Eq. (A5), we have Eqs. (7), (8), (9), and (10).

Under the condition that the thicknesses of all imaginary thin layers are the same, we obtain Eqs. (11) and (12) for F_i and R using the following relations:

$$d_i=d, \tag{A6}$$

$$\sum_{k<i}a_kd_k-\sum_{k<j}a_kd_k+\frac{a_i d_i-a_j d_j}{2}$$

$$=d\left(\sum_{k<i}a_k-\sum_{k<j}a_k+\frac{a_i-a_j}{2}\right), \tag{A7}$$

$$2\sum_{j<i}d_j+d_i=2(i-1)d+d=(2i-1)d. \tag{A8}$$

[1] R. H. Saul, J. Appl. Phys. **40**, 3273 (1969).
[2] F. K. Reinhard and R. A. Logan, J. Appl. Phys. **44**, 3171 (1973).
[3] G. H. Olsen and M. Ettenberg, J. Appl. Phys. **48**, 2543 (1977).
[4] H. Shimizu, K. Itoh, M. Wada, T. Sugino, and I. Teramoto, IEEE J. Quantum Electron. **QE-17**, 763 (1981).
[5] Z. Feng and H. Liu, J. Appl. Phys. **54**, 83 (1983).
[6] S. N. G. Chu, A. T. Macrander, K. E. Strege, and W. D. Johnston, Jr., J. Appl. Phys. **57**, 249 (1985).
[7] F. Cembali and M. Servidori, J. Appl. Cryst. **22**, 345 (1989).
[8] N. N. Davidenkov, Sov. Phys. Solid State **2**, 2595 (1961).
[9] K. Nakajima, J. Cryst. Growth **113**, 477 (1991).
[10] W. A. Brantley, J. Appl. Phys. **44**, 534 (1973).
[11] T. B. Bateman, J. Appl. Phys. **30**, 544 (1959).
[12] R. Reifenberger, J. Appl. Phys. **40**, 5403 (1969).
[13] F. S. Hickernell and W. R. Gayton, J. Appl. Phys. **37**, 462 (1966).
[14] G. Giesecke and H. Pfister, Acta Crystallogr. **11**, 369 (1958).
[15] L. R. Weisberg and J. Blanc, J. Appl. Phys. **34**, 1002 (1963).
[16] R. Bisaro, P. Merenda, and T. P. Pearsall, Appl. Phys. Lett. **34**, 100 (1979).
[17] E. D. Pierron, D. L. Parker, and J. B. McNeeley, J. Appl. Phys. **38**, 4669 (1967).